IEEE Access
Multidisciplinary ⋮ Rapid Review ⋮ Open Access Journal

Received 22 April 2024, accepted 12 May 2024, date of publication 27 May 2024, date of current version 10 June 2024.

Digital Object Identifier 10.1109/ACCESS.2024.3405401

RESEARCH ARTICLE

Sensor-Less Drive of Ultra-Low Inductance SPMSM With DC-Link Single Current Sensor

JUN-SIK HWANG, (Student Member, IEEE), MIN-SEOK CHAE, (Student Member, IEEE), AND HYEON-GYU CHOI, (Member, IEEE)
Department of Electrical Engineering, Incheon National University, Incheon 22012, South Korea
Corresponding author: Hyeon-Gyu Choi (hg.choi@inu.ac.kr)

This work was supported by the Incheon National University Research Grant in 2022.

ABSTRACT This article presents a single current sensing method that achieves minimal current reconstruction errors, even at extremely low-speed region. In vector control applications, a drive system that combines single current sensor with position sensorless techniques is attractive as it minimizes the use of sensors. The current reconstruction method using the DC current measurement method introduces current reconstruction errors because of the sampling timing of single current sensor method. Moreover, current dc current measurement method has a dead zone where current reconstruction is not possible, leading to pronounced current ripple during the avoidance process. In the case of ultra-low inductance motors, the increase in current ripple exacerbates the drive performance, especially at low speeds. When the single current sensor method and sensorless drive are applied to an ultra-low inductance non-salient pole synchronous motor, it can lead to operational failures due to high current ripple and current reconstruction errors at low-speed region. This article proposes a technique to improve the performance in the low-speed region when current reconstruction method using dc current sensor and sensorless techniques are used together by eliminating dead zone in the low-speed region minimizing current reconstruction errors with a model-free method. The current reconstruction performance, sensorless startup, and operation performance have verified through experiments.

INDEX TERMS Current measurement, AC motors, motor drives, sensorless control, voltage source inverters.

I. INTRODUCTION

Permanent magnet synchronous machine (PMSM) are widely used due to their high torque density, high efficiency, and its stability. When controlling PMSM, voltage source inverters (VSI) are commonly used to implement control using pulse width modulation (PWM) techniques. Systems utilizing VSI-PWM results in lower switching ripple and higher performance compared to other digital drive techniques due to their high dynamic characteristics and steady-state stability. To achieve stable and high-performance control of PMSM, it is essential to accurately measure the phase current and the rotor angle. Typically, for vector control of PMSM, it is necessary to have at least one angle sensor such as an encoder or resolver, and a minimum of two current sensors such as hall effect current sensors. The use of such sensors results in increased costs and size. So, reducing the number of sensors in PMSM drive systems has been extensively researched due to advantages such as cost reduction and circuit miniaturization.

Over the past few decades, research has been conducted on current reconstruction techniques using a single current sensor (SCS) in the dc stage, as shown in Fig. 1, to reduce the number of current sensors [1], [2], [3], [4], [5], [6]. When

The associate editor coordinating the review of this manuscript and approving it for publication was Zhuang Xu.

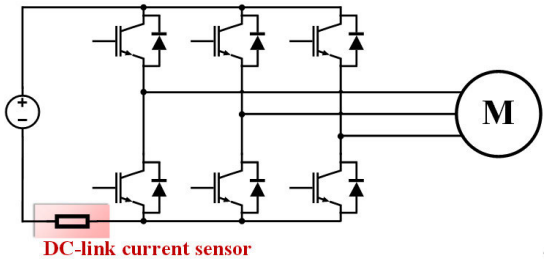

FIGURE 1. A 3-phase inverter utilizing position sensorless operation and a DC single current sensor.

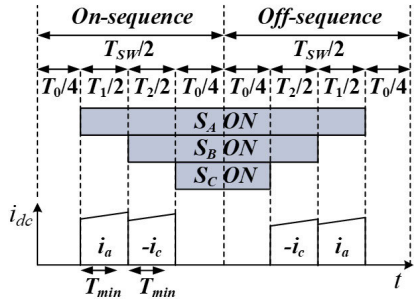

FIGURE 2. Switching wave of 3-phase inverter and current wave of dc current wave. (MI = 0.5, $\theta_r = \frac{\pi}{3}$).

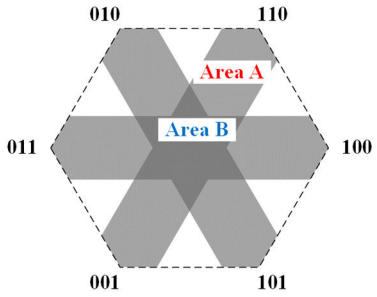

FIGURE 3. Phase current immeasurable area of a SCS inverter.

using SCS method, the phase current can only be sampled in the active voltage vectors as shown in Fig. 2. S_A, S_B, S_C represent the signals for the high-side switch of each phase. 1 represents the on-state of the switch, while 0 denotes the off-state of switch. Each active voltage vector should last longer than the minimum current sampling latency ($T_{\min}$). $T_{\min}$ includes settling time of the current, inverter dead time, and the time it takes for the analog-to-digital converter to sample. This constraint generates a current reconstruction dead zone (CRDZ) where current cannot be reconstructed as shown in Fig. 3. CRDZ occurs in the sector boundary region (Area A in Fig. 3), where only one phase current can be measured, and in the low modulation region (Area B in Fig. 3) where no phase current can be measured at all. In addition, when employing the Space Vector PWM (SVPWM) method for switching, there exists current reconstruction error due to the timing of current sampling [7].

To overcome such issues, techniques for reconstruction phase current using SCS have been studied through various methods. In [8] and [9], techniques for injecting measurement voltage to ensure $T_{\min}$. These methods still have current reconstruction errors and perform poorly in the low-speed region. In [10], [11], [12], and [13], observer-based techniques for current reconstruction are introduced. These methods offer the advantage of reconstructing current without current reconstruction errors. However, they come with the drawback of performance degradation when parameters vary and the limitation that accurate reconstruction is only possible when the phase current is pure sine wave.

TABLE 1. Relation between DC current and phase current depending on the switching state.

Switching states (S_A, S_B, S_C)	Current relation
(0, 0, 0) / (1, 1, 1)	Not available
(1, 0, 0)	$i_{dc} = i_a$
(0, 1, 0)	$i_{dc} = i_b$
(0, 0, 1)	$i_{dc} = i_c$
(1, 1, 0)	$i_{dc} = -i_c$
(0, 1, 1)	$i_{dc} = -i_a$
(0, 0, 1)	$i_{dc} = -i_b$

In addition to SCS methods, position sensorless control techniques have also been widely researched for AC drive systems with reduced sensor. One of the widely used methods is estimating the angle of the motor by using back electromotive force (BEMF) [14], [15], [16]. This method involves utilizing a BEMF observer to estimate the rotor angle. However, BEMF tends to have low values at low speeds, which leads to poor performance at low-speed region. In the case of salient-pole electric machines, there is a technique that estimates the rotor angle by tracking the saliency of rotor through high-frequency injection [17], [18], [19]. This method can estimate the angle in all regions, including low-speed region. However, it generates additional noise and, crucially, is not applicable to non-salient-pole machines like surface mounted PMSM (SPMSM). Therefore, when sensorless operation is required for non-salient-pole machines, we initially operate in an open-loop control [20], [21]. Once a sufficient speed for angle estimation with BEMF is reached, they transition into sensorless operation.

When driving PMSMs, the use of a single current sensor and sensorless algorithms is advantageous for cost and size reduction in applications, so it is widely adopted. Particularly in home appliance systems such as vacuum cleaners and air conditioner compressors have particular requirements for low cost and compact size. Some systems also demand high-speed operation of tens of thousands of RPM or more. To meet these requirements, ultra-low inductance motors are utilized, along with the adoption of SCS and sensorless positioning techniques. Additionally, in recent times, SCS and sensorless positioning techniques are widely applied in systems such as electric vehicle cooling pump motors. Using non-salient pole motors like SPMSMs in such systems can be critical in the low-speed operating range due to the measurement errors of SCS. Conventional single DC current sensor methods suffer from current reconstruction errors due to the different current measurement timing of SCS, exacerbating the issue with

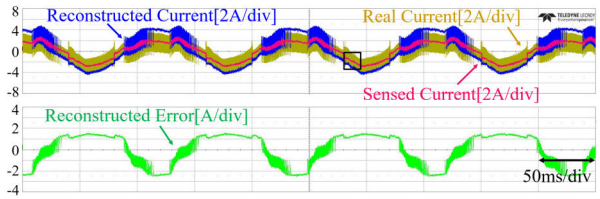

FIGURE 4. Waveforms of phase current and reconstructed error by the conventional method with SVPWM when operating condition is rated torque at 500r/m.

TABLE 2. Parameters of PMSM.

	Symbol	Value	Unit
DC-link voltage	V_{dc}	15	V
Number of poles	P	2	-
Phase resistance	R_s	0.26	Ω
d-axis inductance	L_d	31	μH
q-axis inductance	L_q	31	μH
Rotor flux linkage	λ_{PM}	0.0072	V·s
Rated RMS current	$I_{s,RMS,rated}$	4.0	A_{rms}
Rated power	-	55	W
Rated speed	-	20000	r/min
Switching frequency	f_{sw}	30	kHz
Sampling frequency	f_{samp}	30	kHz

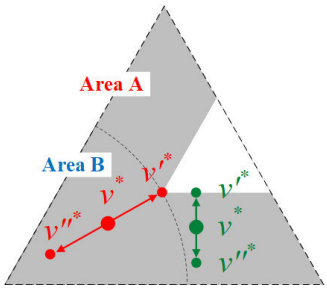

FIGURE 5. Phase current immeasurable area of a SCS inverter.

ultra-low inductance motors which has large current ripples. Therefore, this presents a significant constraint on initial startup. To secure sensorless performance during low-speed operation, some systems use Interior Permanent Magnet Synchronous Machines (IPMSMs). However, due to their higher manufacturing costs compared to SPMSMs, they are not suitable for low-cost systems.

To address the significant performance degradation in the low-speed region when using both the SCS method and sensorless operation, this paper proposes a novel approach using SCS, introducing new PWM strategy and current reconstruction techniques. The proposed approach eliminates CRDZ at low-speed region and enables the reconstruction of phase current from zero to medium speed range without the need for any voltage injection. Furthermore, it theoretically minimizes phase current reconstruction errors to zero, resulting in minimal position sensorless operation errors related to BEMF estimation and thus enhancing sensorless control performance in low-speed region.

The adoption of this technique allows for the extension of the sensorless operation range of systems utilizing both SCS and sensorless techniques to even lower speeds. Furthermore, improvements in the performance of sensorless operation itself can be expected. This implies that SPMSMs can now be operated under more adverse conditions than before, paving the way for cost-effective and compact-sized production in industries utilizing such systems.

In Section II, the conventional single current sensor method is described. Section III describes the new single shunt technique using the switching signal split method. Section IV examines experimental results to verify the feasibility and superiority of the proposed approach by comparing with the conventional SCS method. Finally, Section V concludes the discussion.

II. CONVENTIONAL SINGLE CURRENT SENSOR TECHNOLOGIES

When using SCS method to reconstruct the phase as shown in Fig. 1, it is possible to sample the phase current through SCS only when the active voltage vector is being applied.

In the conventional SVPWM switching method, two zero voltage vector intervals and two different active voltage vector intervals are applied within one switching cycle. After sampling i_{dc} for each active voltage vector, the i_{dc} is matched to the phase current according to Table 1. Through the above process, it is possible to reconstruct the currents of two phases in one switching cycle, and the remaining phase current can be calculated by (1). This allows the reconstruction of three-phase currents in each switching cycle.

$$i_a + i_b + i_c = 0 \tag{1}$$

This method has the advantage of reconstructing phase currents with minimal voltage injection, resulting in good harmonic characteristics [8]. However, there are several issues associated with this approach. The first challenge is inability to sample the average value of the phase current. In the conventional SVPWM switching method, sampling the phase current at the midpoint of the zero vector allows sampling the average current value [7]. However, as shown in Fig. 2, since i_{dc} is 0 in the zero-voltage vector, it is impossible to sample average current value using SCS. It leads to consistent reconstruction errors as shown in Fig. 4. The motor parameters are listed in Table 2.

Another challenge is the voltage distortion that occurs when avoiding CRDZ. As shown in Fig. 5, when the inverter voltage reference v^* is within the CRDZ, additional voltage is injected during half switching cycle to apply the modified voltage reference v'^*. Meanwhile, current is sampled through SCS during this period. Afterward, voltage reference v''^*, opposite to v'^*, is applied to compensate for the voltage reference v^*. The injection of voltage leads to additional current ripple, as expressed in the (2), where Ra, La: stator winding resistance, inductance, i_d^r, i_q^r: dq-axis stator current of rotor reference frame, v_d^r, v_q^r: dq-axis stator voltage of rotor reference frame, θ_r,ω_r: electrical angle and speed of the rotor,

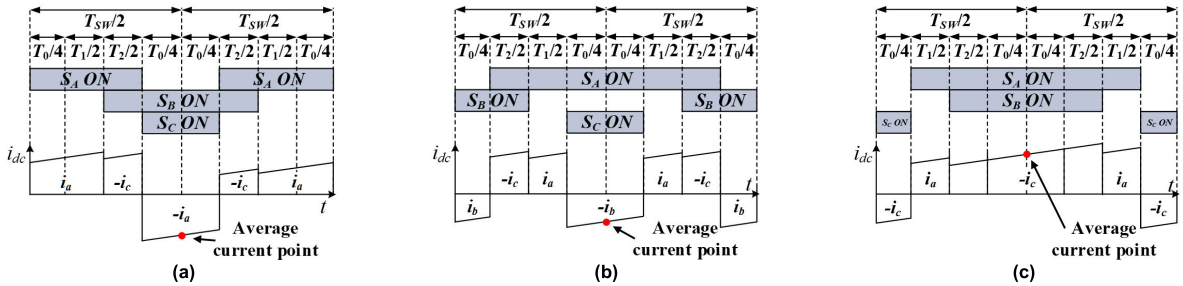

FIGURE 6. The switching waveforms when applying the SSS method. The red dots represent the average current value. (MI = 0.5, $\theta_r = \frac{\pi}{3}$) (a) apply to the SSSPWM-1. (b) apply to the SSSPWM-2. (c) apply to the SSSPWM-3.

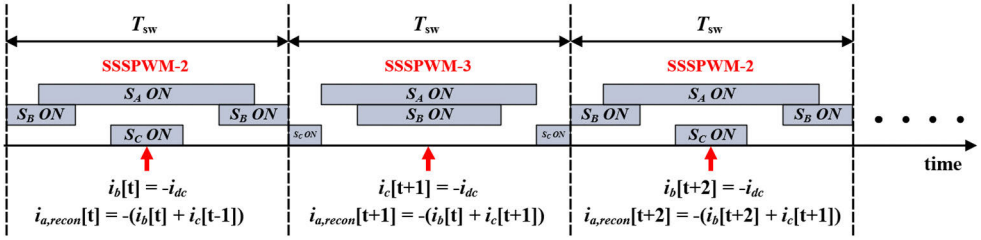

FIGURE 7. Example of average phase current reconstruction strategy using SSSPWM. (MI = 0.5, $\theta_r = \frac{\pi}{3}$).

and ω_{sw}: switching frequency [22].

$$\begin{bmatrix} \Delta i_d^r \\ \Delta i_q^r \end{bmatrix} = \frac{1}{(R_s + j\omega_{sw}L_s)^2 + L_s^2\omega_r^2} \times \begin{bmatrix} R_s + j\omega_{sw}L_s & L_s\omega_r \\ -L_s\omega_r & R_s + j\omega_{sw}L_s \end{bmatrix} \times \begin{bmatrix} \Delta v_d^s \cos\theta_r + \Delta v_q^s \sin\theta_r \\ -\Delta v_d^s \sin\theta_r + \Delta v_q^s \cos\theta_r \end{bmatrix} \quad (2)$$

To avoid CRDZ, more voltage injection is required in the low-speed region, represented as Area B in Fig. 5, compared to Area A in the same figure. Consequently, this leads to an increased current ripple at low-speed region. Especially in ultra-low inductance PMSMs, this problem is worsened because the low inductance causes a huge current ripple even with very small voltage injection by (2).

III. SINGLE CURRENT SENSOR TECHNOLOGIES REDUCING RECONSTRUCTION ERROR

In this section, a technique is introduced that modifies the PWM to enable switching without zero voltage vectors and accurately samples the average current value using SCS. This aims to eliminate CRDZ in the low-speed region, enabling current reconstruction without any voltage injection in that specific operating range. And it achieves current reconstruction without errors between the reconstructed phase current and average value of phase current. And it proposes an offset voltage for extending the reconstructible region of the proposed method.

TABLE 3. Relation between dc current and phase current depending on the proposed method.

Mode of SSS method	Current relation
SSSPWM-1	$i_{dc} = -i_{max}$
SSSPWM-2	$i_{dc} = -i_{mid}$
SSSPWM-3	$i_{dc} = -i_{min}$

A. PWM STRATEGY FOR ELIMINATING AT LOW-SPEED REGION

When dividing one of the three-phase signals in SVPWM at the beginning and end of the switching cycle, the switching waveform changes as shown in Fig. 6. As seen in Fig. 6, by Switching Signal Split PWM(SSSPWM), it is possible to measure the phase current at the midpoint of the switching cycle via SCS, and the measured phase current at this time represents the average current value.

At the sampling point depicted in Fig 6, accurately measuring the average phase current can be achieved by sampling the DC link current. However, in practical systems, there might be a delay from the generation of the start-of-conversion (SOC) signal to the actual sampling process. This delay can result in the sampling occurring at a point later than the sampling point illustrated in Fig 6, which could lead to measurement errors in the SCS method. In such scenarios, adjusting the SOC signal to occur earlier, considering the actual system delay, becomes necessary to ensure accurate measurement of the average phase current.

A similar switching technique to SSSPWM has already been studied as a strategy to reduce the common mode voltage of an electric machine by replacing zero vectors

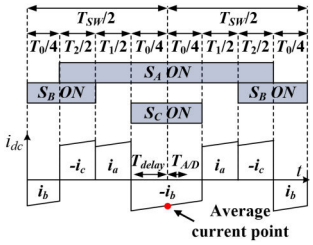

FIGURE 8. The time required to secure for average current measurement.

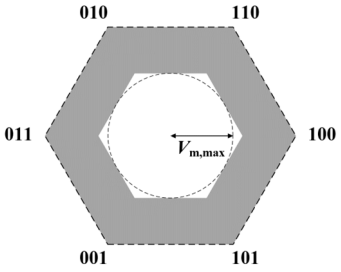

FIGURE 9. Current reconstruction dead zone of proposed SSS method.

with active vectors [23]. In this section, in addition to the SSSPWM switching strategy, additional strategies are presented to propose a technique for three-phase current reconstruction with theoretically zero reconstruction error using SCS.

This paper refers to the splitting of the phase associated with $v^*_{\max}$ as SSS-1, the application to v^*_{mid} as SSS-2, and the application to $v^*_{\min}$ as SSSPWM-3. $v^*_{\max}$ represents the maximum value among the phase voltage reference, $v^*_{\min}$ represents the minimum value, and v^*_{mid} represents the midpoint value. The relationship of sampled phase currents in each mode is depicted in Table 3. $i_{\max}$ represents the phase current of the $v^*_{\max}$ phase, i_{mid} is the phase current of the v^*_{mid} phase, and $i_{\min}$ is the phase current of the $v^*_{\min}$ phase. By employing SSSPWM, measuring the DC current at the midpoint of the switching cycle enables the measurement of the average current value of one phase per switching cycle. As depicted in Fig. 7, by alternately applying SSSPWM1-3 at each switching cycle (e.g., SSSPWM-2 -> SSSPWM-3 -> SSSPWM-2 ...), it is possible to reconstruct the average current values of the three phases.

In the proposed method of this paper, to measure the current using SCS, it is necessary to ensure that there is sufficient time for current measurement from the current measurement point to the switching occurrence point as shown in Fig. 8. T_{delay} represents the sum of the inverter dead time and the settling time of the dc current and, $T_{A/D}$ represents the time required for the analog-to-digital converter to sample the dc current value. In SSSPWM, the duration of the voltage vectors where current measurement occurs is equivalent to the duration of the zero voltage vectors T_0 in conventional SVPWM. Therefore, the current reconstruction method depicted in Fig. 8 is capable of reconstructing current in the medium to low-speed range where T_0 is sufficiently ensured. The condition for current measurement feasibility is given as (3).

$$\begin{cases} \dfrac{T_0}{2} > 2T_{\text{delay}} & (T_{\text{delay}} > T_{A/D}) \\ \dfrac{T_0}{2} > 2T_{A/D} & (T_{\text{delay}} < T_{A/D}) \end{cases} \tag{3}$$

Since the duration of the central vector where current measurement occurs in SSSPWM is equivalent to the duration of the zero-voltage vector in SVPWM, the relationship between the duration T_0 of the zero-voltage vector and the magnitude of the voltage reference of the inverter is given by (4) [24], [25], [26].

$$T_0 = T_{sw}(1 - \frac{\sqrt{3}V^*}{V_{\text{DC}}}) \tag{4}$$

By substituting (4) into (3), we can determine the maximum range of voltage reference magnitude for which current reconstruction is feasible, as shown in (5) and Fig. 9.

$$\begin{cases} V_{\text{m,max}} < \dfrac{V_{\text{DC}}}{\sqrt{3}}(1 - 4f_{sw}T_{\text{delay}}) & (T_{\text{delay}} > T_{A/D}) \\ V_{\text{m,max}} < \dfrac{V_{\text{DC}}}{\sqrt{3}}(1 - 4f_{sw}T_{A/D}) & (T_{\text{delay}} < T_{A/D}) \end{cases} \tag{5}$$

B. OFFSET VOLTAGE COMPENSATION FOR EXTENDING CURRENT RECONSTRUCTIBLE REGION

In the previous section, a switching strategy for sampling the average current value using the SCS was introduced. Furthermore, we have also derived the maximum magnitude of voltage commands for which current reconstruction is feasible using this method. If an appropriate offset voltage reference is applied to phase voltage references, the proposed method can reduce CRDZ. Therefore, in this section, we derive an offset voltage reference that can reduce CRDZ in the proposed method and introduce a sampling strategy for the DC current.

The conditions to expand the current reconstruction region are as follows.

1. The duration for applying the current sampling vector (centered effective vector) must be maximized.

2. The split-phase switching should not occur during the on-time of the centered effective vector.

As shown in Fig. 10, if the combined switch-on times of the midpoint terminal voltage ($v^*_{\text{mid}} + v^*_{sn}$) and the minimum terminal voltage ($v^*_{\min} + v^*_{sn}$) phases equal the switching period and alternating between SSSPWM-2 and SSSPWM-3, the current reconstruction available region of a single current sensor would be maximized.

In this case, the offset voltage can be derived as (6)-(8) [27].

$$(v^*_{\text{mid}} + v^*_{sn}) + (v^*_{\min} + v^*_{sn}) = 0 \tag{6}$$

$$v^*_{sn} = -\frac{v^*_{\text{mid}} + v^*_{\min}}{2} \tag{7}$$

$$if\ , v^*_{\max} + v^*_{sn} \geq \frac{V_{DC}}{2} \Rightarrow v^*_{sn} = \frac{V_{DC}}{2} - v^*_{\max} \tag{8}$$

When applying the offset voltage in (7), with the SSSPWM-2 and SSSPWM-3 methods, the time available for

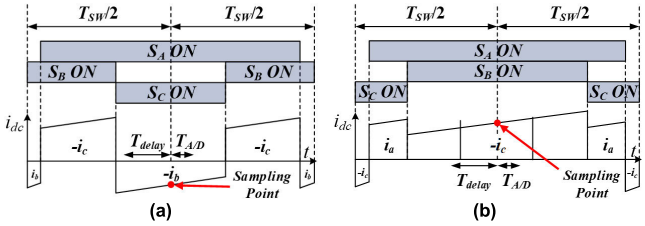

FIGURE 10. The switching waveforms when applying the SSS method with proposed offset voltage. (MI = 0.5, $\theta_r = \frac{\pi}{3}$) (a) apply to the SSSPWM-2. (b) apply to the SSSPWM-3.

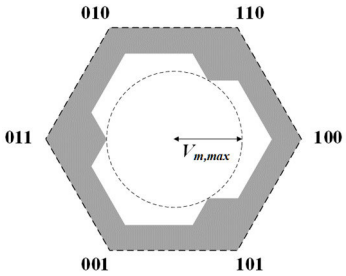

FIGURE 11. Current reconstruction dead zone of proposed SSS method with proposed offset voltage reference.

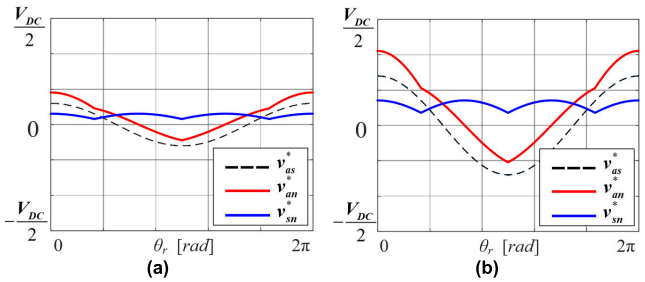

FIGURE 12. The waveforms of the offset voltage reference (blue), terminal voltage reference (red), and phase voltage reference (dotted) for phase A. (a) MI = 0.2. (b) MI = 0.5.

sampling the average current value can be extended, as shown in Fig. 10.

Adding the offset voltage reference from (7) to the phase voltage references, the condition for current measurement becomes as shown in (9).

$$\begin{cases} T_{v_{\min}} + T_{\text{offset}} \geq 2T_{\text{delay}} & (\text{if}, \quad T_{\text{delay}} > T_{\text{A/D}}) \\ T_{v_{\min}} + T_{\text{offset}} \geq 2T_{\text{A/D}} & (\text{if}, \quad T_{\text{A/D}} > T_{\text{delay}}) \end{cases} \tag{9}$$

The relationship between the magnitude of the terminal voltage reference obtained by adding the offset voltage reference to the minimum phase voltage reference and the switching application time is given by (10) [24], [27].

$$T_{v_{\min}} + T_{\text{offset}} = \left(\frac{v^*_{\min} + v^*_{\text{offset}}}{V_{\text{DC}}} + 0.5\right) T_{sw} \tag{10}$$

Adding the offset voltage reference from (5) to the minimum phase voltage reference yields a value of (11). Then, from (9) to (11), maximum magnitude of voltage reference for which current reconstruction is feasible can be derived,

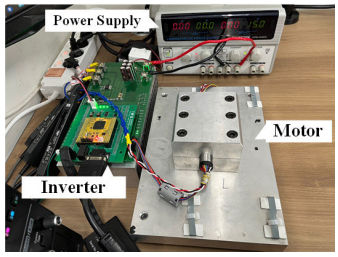

FIGURE 13. Experimental setup.

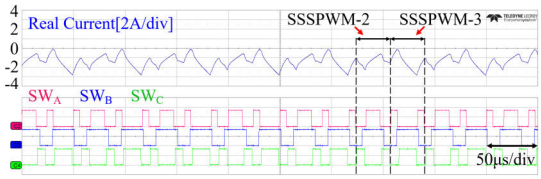

FIGURE 14. Phase current and switching waveform of proposed method.

as shown in (12) and Fig 11.

$$v^*_{\min} + v^*_{\text{offset}} = -\frac{3}{4}V_m \quad (\text{if}, \ \theta_r = \frac{\pi}{3} \text{ or } \theta_r = \pi \text{ or } \theta_r = \frac{5\pi}{3}) \tag{11}$$

$$\begin{cases} V_{\text{m,max}} = -\frac{4}{3}V_{\text{DC}}(2T_{\text{delay}}f_{sw} - 0.5) & (\text{if}, \quad T_{\text{delay}} > T_{\text{A/D}}) \\ V_{\text{m,max}} = -\frac{4}{3}V_{\text{DC}}(2T_{\text{A/D}}f_{sw} - 0.5) & (\text{if}, \quad T_{\text{A/D}} > T_{\text{delay}}) \end{cases} \tag{12}$$

Additionally, the terminal voltage reference and offset voltage reference under these conditions are shown in Fig. 12. The proposed offset voltage reference contains the 6th harmonic component and DC component. So, there is no influence of harmonic distortion due to the offset voltage in the case of three-phase balanced motor.

IV. EXPERIMENTAL RESULTS

This section demonstrates the proposed current reconstruction method and control performance of the proposed SCS drive with BEMF sensorless algorithm. The experimental setup is depicted in Fig. 13, and a two coupled ultra-low inductance SPMSMs and two three-phase inverters with Si-MOSFET was utilized. The inverter was controlled using the TMS320C28346 DSP from Texas Instruments with a system clock of 300MHz. The bandwidths of the speed controller and current controller were set as 10Hz and 500Hz, respectively. A 1.5mΩ shunt resistor and a current sense amplifier with a bandwidth of 750MHz were employed with SCS. The $T_{\min}$ for the experimental setup is 4.0 μs ($T_{\text{delay}} = 3.5$ μs, $T_{\text{A/D}} = 0.5$ μs). For the target motor, control was exclusively implemented based on the dc current measurement only, rotary encoder and phase current sensors only employed for monitoring.

Fig. 14 shows the phase current and switching waveforms when the proposed method is applied. As explained in the

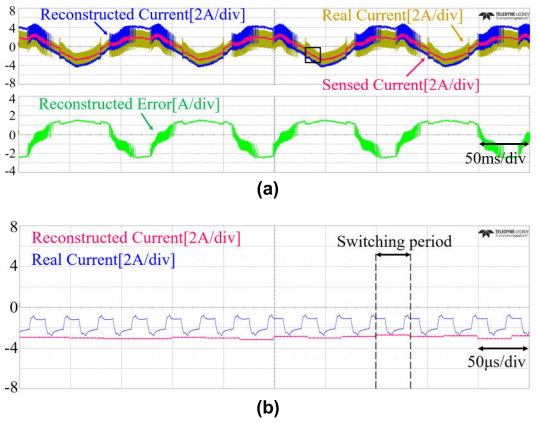

FIGURE 15. Waveforms of sensed, reconstructed, and real phase current and current reconstructed error. Control command is 500r/min, 4A with conventional SCS method. (a) entire waveform. (b) Zoomed waveform.

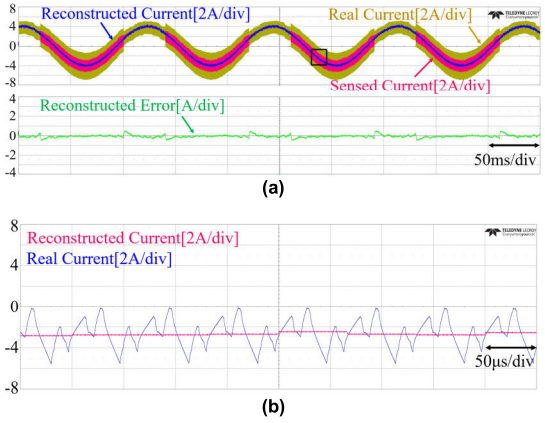

FIGURE 16. Waveforms of sensed, reconstructed, and real phase current and current reconstructed error. Control command is 500r/min, 4A with proposed SCS method. (a) entire waveform. (b) Zoomed waveform.

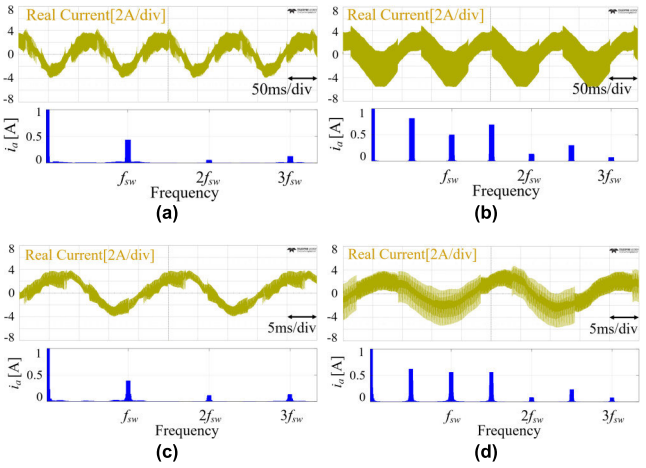

FIGURE 17. Phase currents and their FFT results according to the PWM method. (a) 500rpm conventional method (b) 500rpm SSS method (c) 3000rpm conventional method (d) 3000rpm SSS method.

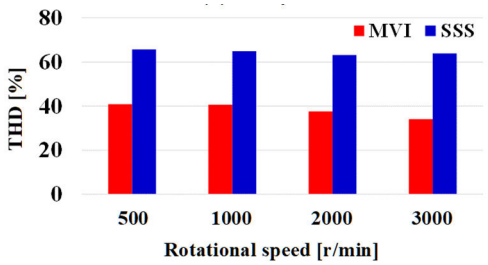

FIGURE 18. THD results of phase current according to operating speed and SCS method. Phase current is $2A_{rms}$.

previous section, it can be observed that SSSPWM-2 and SSSPWM-3 are repeatedly applied every switching cycle.

In the comparison experiments for current reconstruction, Ha's Minimum Voltage Injection(MVI) method [8], widely used for its favorable THD characteristics, was employed.

Fig. 15 and 16 illustrate the steady-state current reconstruction performance at 500r/m. The motor was controlled to generate the rated torque. Fig. 15-(a) and 16-(a) show the actual current, the current obtained from the current sensor, the reconstructed current, and the current reconstruction error. And Fig. 15-(b) and 16-(b) show a part of the waveform shown in Fig. 15-(a) and 16-(a). To evaluate the reconstruction accuracy, the reconstructed current was compared to the sensed current using a phase current sensor. In the case of the conventional SCS method, the current reconstruction error is approximately 4A peak-to-peak, whereas in the proposed method, it can be observed that the current reconstruction error is about 0.8A peak-to-peak.

The switching ripple was also compared at different speed ranges. Fig. 17-(a) and (c) show the phase currents and FFT results when operated at 500 and 3000 r/min using the conventional SCS method. Fig. 17-(b) and (d) show the phase currents and FFT results when operated at 500 and 3000 r/min using the proposed method. The phase currents were operated at $2A_{rms}$ for all cases. Compared to the conventional SCS method, where the ripple component dominates at the switching frequency f_{sw}, the proposed method includes half of the switching frequency component in the current ripple. And the THD results for each operating region are compared in Fig. 18. The THD of phase current in the proposed method increased by approximately 59.7% in the region below 1000 r/min compared to the conventional MVI method, and it increased by over 65% in the region above 1000 r/min. Compared to the conventional MVI method, which shows good THD performance due to the minimum voltage injection for current reconstruction, the proposed method demonstrates an increase in switching ripple due to the change in PWM strategy. To investigate the impact of current reconstruction errors on sensorless algorithms, sensorless startup experiments were conducted using both the proposed method and the conventional method. Fig. 19-21 depict the experimental results, including the real rotor angle, estimated rotor angle, angle estimation error, estimated rotor speed, and three-phase real currents of the motor. The motor was initially started with I-F operation, and the control transitioned from the target speed to vector control using the

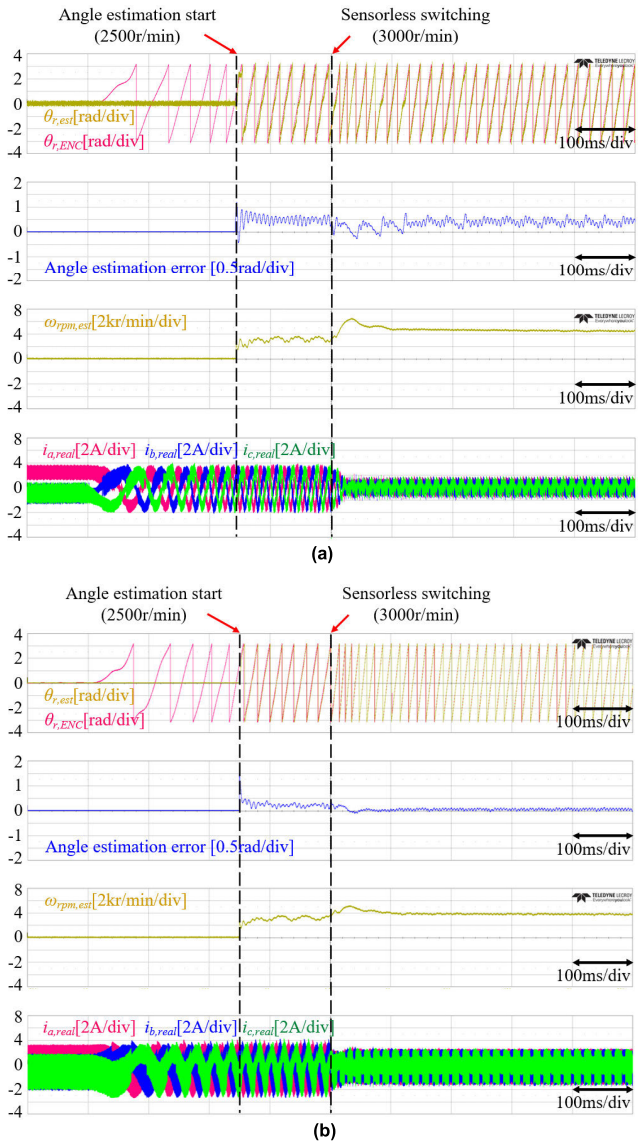

FIGURE 19. Sensorless transition and operation performance at 15% of rated speed (3000 r/min). (a) Operation with the conventional SCS method. (b) Operation with the proposed SCS method.

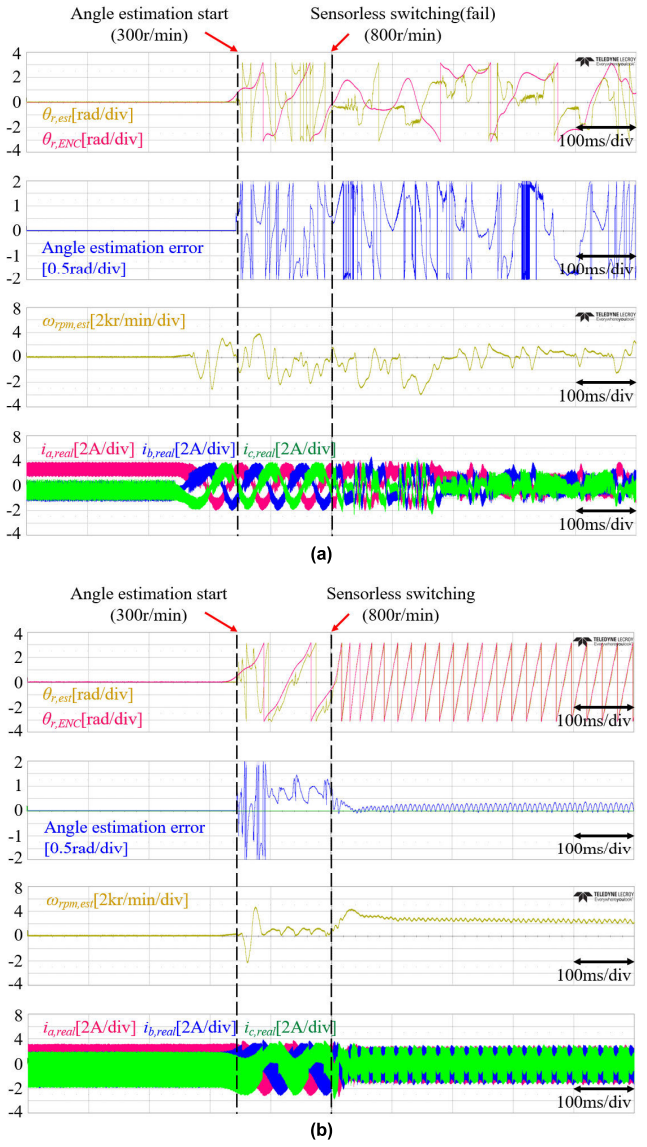

FIGURE 20. Sensorless transition and operation performance at 4% of rated speed (800 r/min). (a) Operation with the conventional SCS method. (b) Operation with the proposed SCS method.

estimated angle. Angle estimation began 500r/min below the target speed. Fig. 19 shows the experimental results at a target speed of 3000 r/min, which is 15% of the rated speed. Starting angle estimation from 2500 r/min and transitioning to vector control at 3000 r/min. Fig. 19-(a) represents the result of the conventional SCS method, while Fig. 19-(b) illustrates the experimental result of the proposed method. Both methods successfully transition to vector control. But, in the case of the conventional SCS method, an angle estimation error is approximately 0.7 radians before transitioning to vector control, whereas the proposed method shows an angle estimation error around 0.3 radians. Due to the larger angle estimation error in the conventional SCS method, there is a significantly larger speed overshoot during the transition to vector control compared to the proposed method. Furthermore, after transitioning to vector control, the proposed method converges to nearly zero angle estimation error, while the conventional method remains an angle estimation error of about 0.6 radians even during vector control.

TABLE 4. Minimum speed for sensorless operation according to SCS method.

Method of SCS	Minimum speed for sensorless operation [r/min]
Minimum Voltage Injection	2500
Switching Signal Split	800

If the transition to vector control is made at a lower speed, the difference becomes more pronounced. Fig. 20 depicts the experimental waveform with the target speed set to 4% of the rated speed, which is 800 r/min. Starting angle estimation from 300 r/min and transitioning to vector control at 800 r/min. As shown in Fig. 20-(a), in the case of the conventional SCS method, angle estimation did not proceed

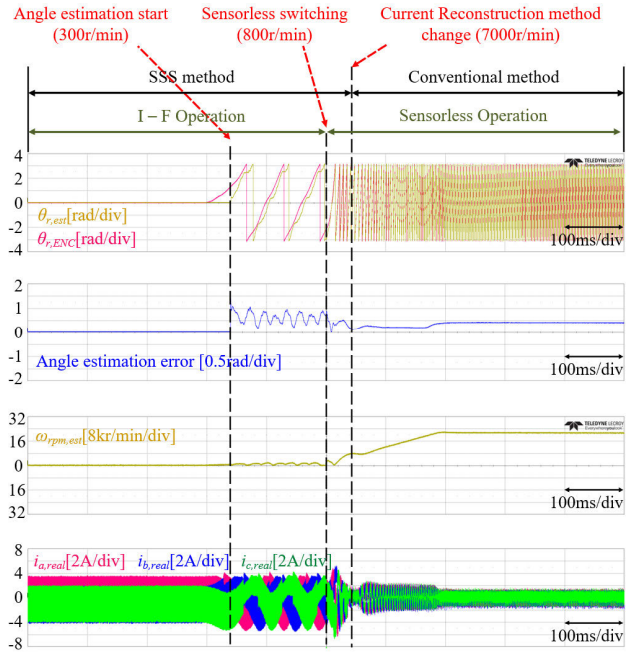

FIGURE 21. Experimental results showing the transition from the initial startup using the SSS method to the conventional SCS method at 7kr/min, reaching the rated speed.

successfully. Therefore, it can be observed that sensorless operation failed.

However, with the proposed method, it can be confirmed from Fig. 20-(b) that angle estimation is successful even at 800 r/min, which is 4% of the rated speed. Additionally, the transition to vector control is also successful. The minimum speeds for sensorless operation according to SCS methods are shown in Table 4. When controlling using the conventional SCS method, vector control is achievable in areas exceeding 12% of the rated speed. In contrast, the proposed method allows vector control in areas exceeding 4% of the rated speed.

The proposed method clearly exhibits larger switching ripple compared to the conventional method. However, with the low angle estimation error, the proposed SCS method enables more accurate MTPA operation. Moreover, it has the advantage of quickly entering vector control. Therefore, with the proposed SCS method, the startup reliability can be enhanced.

Fig. 21 illustrates the experimental results of initially starting with the proposed SCS method and transitioning to the conventional SCS method as the rotational speed increases. The motor speed command is 20 kr/min. The motor operated in I-F control with a speed slope of 10kr/min/sec up to 800 r/min, then transitioned to vector control with a slope of 100 kr/min/sec, and switched to conventional SCS method when reaching 7 kr/min.

V. CONCLUSION

This paper has demonstrated a current reconstruction method with minimal current reconstruction error in the low-speed region of an ultra-low inductance PMSM without voltage injection, using a single current sensor. By splitting the switching signals, it is possible to sample the average current value of phase current from the dc current. Taking advantage of this, the proposed method suggests a switching strategy and offset voltage, enabling the reconstruction of three-phase current without current reconstruction errors in low-speed region. Through experiment, this paper demonstrates that the proposed SCS method can reduce the current reconstruction error in the low-speed region by about 80% compared to the conventional method. As a result, it enables sensorless operation of the SPMSM at even lower speeds compare to the conventional SCS method. Furthermore, it has been demonstrated that transition between the conventional SCS method and the proposed method is possible with respect to the speed.

When disturbances or noise occur in the current measurement of SCS, the proposed SCS method may also experience current restoration errors. However, in the case of conventional SCS methods, if current measurement disturbances amplify existing current restoration errors, it can potentially lead to critical issues. On the other hand, with the proposed SCS method, errors due to measurement disturbances are added to the average current value, making it less critical compared to conventional SCS methods.

In the future, in the mid to high-speed range, the superior harmonic characteristics of the conventional SCS method can be utilized. Additionally, intermittent application of the proposed SCS method can be employed to obtain average phase current values, and compensating for current reconstruction errors of the conventional SCS method with the average phase current values. This direction of research allows for the development of additional compensation mechanisms of conventional SCS method.

REFERENCES

[1] J. T. Boys, "Novel current sensor for PWM AC drives," *IEE Proc. B Electr. Power Appl.*, vol. 135, no. 1, p. 27, 1988.
[2] Y. Shen, D. Liu, W. Liang, and X. Zhang, "Current reconstruction of three-phase voltage source inverters considering current ripple," *IEEE Trans. Transport. Electrific.*, vol. 9, no. 1, pp. 1416–1427, Mar. 2023.
[3] C.-M. Wang and S.-K. Lin, "A simple single shunt current reconstruction approach for low-cost permanent magnet synchronous motor drives," in *Proc. Int. Autom. Control Conf. (CACS)*, Nov. 2015, pp. 79–84.
[4] Y.-S. Lai, Y.-K. Lin, and C.-W. Chen, "New hybrid pulsewidth modulation technique to reduce current distortion and extend current reconstruction range for a three-phase inverter using only DC-link sensor," *IEEE Trans. Power Electron.*, vol. 28, no. 3, pp. 1331–1337, Mar. 2013.
[5] W. Wang, H. Yan, Y. Xu, J. Zou, X. Zhang, W. Zhao, G. Buticchi, and C. Gerada, "New three-phase current reconstruction for PMSM drive with hybrid space vector pulsewidth modulation technique," *IEEE Trans. Power Electron.*, vol. 36, no. 1, pp. 662–673, Jan. 2021.
[6] W. Wang, M. Cheng, Z. Wang, and B. Zhang, "Fast switching direct torque control using a single DC-link current sensor," *J. Power Electron.*, vol. 12, no. 6, pp. 895–903, Nov. 2012.
[7] S.-H. Song, J.-W. Choi, and S.-K. Sul, "Current measurements in digitally controlled AC drives," *IEEE Ind. Appl. Mag.*, vol. 6, no. 4, pp. 51–62, Jul. 2000.
[8] J.-I. Ha, "Voltage injection method for three-phase current reconstruction in PWM inverters using a single sensor," *IEEE Trans. Power Electron.*, vol. 24, no. 3, pp. 767–775, Mar. 2009.
[9] H. Kim and T. M. Jahns, "Phase current reconstruction for AC motor drives using a DC link single current sensor and measurement voltage vectors," *IEEE Trans. Power Electron.*, vol. 21, no. 5, pp. 1413–1419, Sep. 2006.

[10] B. Hafez, A. S. Abdel-Khalik, A. M. Massoud, S. Ahmed, and R. D. Lorenz, "Single-sensor-based three-phase permanent-magnet synchronous motor drive system with Luenberger observers for motor line current reconstruction," *IEEE Trans. Ind. Appl.*, vol. 50, no. 4, pp. 2602–2613, Jul. 2014.
[11] B. Saritha and P. A. Janakiraman, "Sinusoidal three-phase current reconstruction and control using a DC-link current sensor and a curve-fitting observer," *IEEE Trans. Ind. Electron.*, vol. 54, no. 5, pp. 2657–2664, Oct. 2007.
[12] T. M. Wolbank and P. E. Macheiner, "Current-controller with single DC link current measurement for inverter-fed AC machines based on an improved observer-structure," *IEEE Trans. Power Electron.*, vol. 19, no. 6, pp. 1562–1567, Nov. 2004.
[13] J.-I. Ha, "Current prediction in vector-controlled PWM inverters using single DC-link current sensor," *IEEE Trans. Ind. Electron.*, vol. 57, no. 2, pp. 716–726, Feb. 2010.
[14] N. Matsui, "Sensorless PM brushless DC motor drives," *IEEE Trans. Ind. Electron.*, vol. 43, no. 2, pp. 300–308, Apr. 1996.
[15] S. Morimoto, K. Kawamoto, M. Sanada, and Y. Takeda, "Sensorless control strategy for salient-pole PMSM based on extended EMF in rotating reference frame," *IEEE Trans. Ind. Appl.*, vol. 38, no. 4, pp. 1054–1061, Jul. 2002.
[16] Y.-C. Son, B.-H. Bae, and S.-K. Sul, "Sensorless operation of permanent magnet motor using direct voltage sensing circuit," in *Proc. Conf. Rec. IEEE Ind. Appl. Conf. 37th IAS Annu. Meeting*, Oct. 2002, pp. 1674–1678.
[17] M. J. Corley and R. D. Lorenz, "Rotor position and velocity estimation for a salient-pole permanent magnet synchronous machine at standstill and high speeds," *IEEE Trans. Ind. Appl.*, vol. 34, no. 4, pp. 784–789, Jul. 1998.
[18] J.-I. Ha and S.-K. Sul, "Sensorless field-orientation control of an induction machine by high-frequency signal injection," *IEEE Trans. Ind. Appl.*, vol. 35, no. 1, pp. 45–51, Jan. 1999.
[19] I. Jun-Hyuk, K. Sang-Il, and K. Rae-Young, "Variable-magnitude voltage signal injection for current reconstruction in an IPMSM sensorless drive with a single sensor," *J. Electr. Eng. Technol.*, vol. 13, no. 4, pp. 1558–1565, 2018.
[20] M. Pacha and S. Zossak, "Improved simple I-F open-loop start-up of PMSM drives without speed or position sensor," in *Proc. IEEE 10th Int. Symp. Sensorless Control Electr. Drives (SLED)*, Sep. 2019, pp. 1–6.
[21] L. I. Iepure, I. Boldea, and F. Blaabjerg, "Hybrid I-f starting and observer-based sensorless control of single-phase BLDC-PM motor drives," *IEEE Trans. Ind. Electron.*, vol. 59, no. 9, pp. 3436–3444, Sep. 2012.
[22] H.-g. Choi, J.-I. Ha, and K. Lee, "Ultra-low inductance PMSM drive using a DC current sensor," *IEEE Trans. Ind. Electron.*, vol. 71, no. 6, pp. 5597–5607, Jun. 2024.
[23] A. M. Hava and E. Ün, "A high-performance PWM algorithm for common-mode voltage reduction in three-phase voltage source inverters," *IEEE Trans. Power Electron.*, vol. 26, no. 7, pp. 1998–2008, Jul. 2011.
[24] J.-S. Kim and S.-K. Sul, "A novel voltage modulation technique of the space vector PWM," *IEEJ Trans. Ind. Appl.*, vol. 116, no. 8, pp. 820–825, Jul. 1996.
[25] H. W. van der Broeck, H.-C. Skudelny, and G. V. Stanke, "Analysis and realization of a pulsewidth modulator based on voltage space vectors," *IEEE Trans. Ind. Appl.*, vol. 24, no. 1, pp. 142–150, Jan. 1988.
[26] K. Zhou and D. Wang, "Relationship between space-vector modulation and three-phase carrier-based PWM: A comprehensive analysis [three-phase inverters]," *IEEE Trans. Ind. Electron.*, vol. 49, no. 1, pp. 186–196, Feb. 2002.
[27] D.-W. Chung, J.-S. Kim, and S.-K. Sul, "Unified voltage modulation technique for real-time three-phase power conversion," *IEEE Trans. Ind. Appl.*, vol. 34, no. 2, pp. 374–380, Mar. 1998.

JUN-SIK HWANG (Student Member, IEEE) received the B.S. degree in electrical engineering from Incheon National University, Incheon, South Korea, in 2024, where he is currently pursuing the M.S. degree in electrical engineering. His current research interests include power electronics and motor control.

MIN-SEOK CHAE (Student Member, IEEE) received the B.S. degree in electrical engineering from Incheon National University, Incheon, South Korea, in 2024, where he is currently pursuing the M.S. degree in electrical engineering. His current research interests include electric machine control and power electronics.

HYEON-GYU CHOI (Member, IEEE) received the B.S. and Ph.D. degrees in electrical and computer engineering from Seoul National University, Seoul, South Korea, in 2014 and 2020, respectively. In 2020, he was a Senior Researcher at Garrett Motion Inc., USA. From 2020 to 2022, he was a Senior Engineer at LG Electronics Company, South Korea. Since 2022, he has been an Assistant Professor with the Department of Electrical Engineering, Incheon National University, Incheon, South Korea. His research interests include power electronics and motor control, especially for the high-speed applications.